

NASA TECHNICAL NOTE



NASA TN D-8527 *e.1*

NASA TN D-8527

LOAN COPY: RET
AFWL TECHNICAL
KIRTLAND AFB,



RELATION OF MORPHOLOGY OF ELECTRODEPOSITED ZINC TO ION CONCENTRATION PROFILE

*Charles E. May, Harold E. Kautz,
and Brian B. Sabo*

*Lewis Research Center
Cleveland, Ohio 44135*





0134234

1. Report No. NASA TN D-8527	2. Government Accession No.	3. Recipient's Catalog No.	
4. Title and Subtitle RELATION OF MORPHOLOGY OF ELECTRODEPOSITED ZINC TO ION CONCENTRATION PROFILE		5. Report Date July 1977	6. Performing Organization Code
7. Author(s) Charles E. May, Harold E. Kautz, and Brian B. Sabo		8. Performing Organization Report No. E-9079	
9. Performing Organization Name and Address National Aeronautics and Space Administration Lewis Research Center Cleveland, Ohio 44135		10. Work Unit No. 506-16	11. Contract or Grant No.
12. Sponsoring Agency Name and Address National Aeronautics and Space Administration Washington, D. C. 20546		13. Type of Report and Period Covered Technical Note	
15. Supplementary Notes		14. Sponsoring Agency Code	
16. Abstract The morphology of electrodeposited zinc was studied with special attention to the ion concentration profile. The initial concentrations were 9-M hydroxide ion and 1.21-M zincate. Current densities were 6.4 to 64 mA/cm ² . Experiments were run with a horizontal cathode which was observed in situ via microscope. The morphology of the zinc deposit was found to be a function of time as well as current density; roughly, the log of the transition time from mossy to large crystalline type deposit is inversely proportional to current density. Probe electrodes indicated that the electrolyte in our cathode chamber was mixed by self-induced convection. However, relatively large concentration gradients of the involved species existed across the boundary layer of the cathode. Analysis of the data suggests that the morphology converts from mossy to large crystalline when the hydroxide activity on the cathode surface exceeds about 12 M. Other experiments show that the pulse discharge technique had no effect on the morphology in our system where the bulk concentration of the electrolyte was kept homogeneous via self-induced convection.			
17. Key Words (Suggested by Author(s)) Battery charging; Alkaline batteries; Dendrites; Moss		18. Distribution Statement Unclassified - unlimited STAR Category 44	
19. Security Classif. (of this report) Unclassified	20. Security Classif. (of this page) Unclassified	21. No. of Pages 33	22. Price* A03

RELATION OF MORPHOLOGY OF ELECTRODEPOSITED

ZINC TO ION CONCENTRATION PROFILE

by Charles E. May, Harold E. Kautz, and Brian B. Sabo*

Lewis Research Center

SUMMARY

The morphology of electrodeposited zinc was studied with special attention to the ion concentration profile. The initial concentrations were 9-molar hydroxide and 1.21-molar zincate. Current densities were 6.4 to 64 mA/cm². Experiments were run with a horizontal cathode which was observed in situ via microscope. The morphology of the electrodeposited zinc metal was found to be a function of time as well as current density. Our present belief is that the difference in zinc morphology is fundamentally due to a difference in the activity of hydroxide ion absorbed on the cathode surface. Above about 12 molar, large crystals form; below 12 molar, small crystals (moss) form.

In our experimental system the direct observation of deposit prohibited the use of asbestos or other porous material in contact with the cathode. Thus, convection was possible and was observed via zinc probe electrodes, which showed no appreciable concentration gradient in the cathode chamber. However, concentration differences did exist between the bulk and the surface layer at the cathode: for zincate, 11 (M/liter)/(A/cm² of current); and for hydroxide ion, about 16 (M/liter)/(A/cm² of current). Moreover, the moss deposit had an apparent thermodynamic activity roughly twice that of the zinc sheet used. Finally, in our experimental system, we detected no effect of pulse discharging when comparison was based on average current.

INTRODUCTION

Today, renewed interest is being shown in the performance of secondary batteries, particularly in improving their cycle life. At the Lewis Research Center, this interest is directed toward the silver-zinc and nickel-zinc batteries. This study is concerned

*Assistant Professor of Physics, Saint Olaf College, Northfield, Minnesota; Summer Faculty Fellow at the Lewis Research Center in 1975 and 1976.

with the effect of pulse discharging during charging on the morphology, concentration profile, and performance of the zinc-alkaline half-cell. It has been reported that this technique (pulse discharging during charging) increases the cycle life of nickel-cadmium and lead-acid batteries (ref. 1).

Moreover, this technique is claimed to improve the morphological growth of metals in electroplating (ref. 2) as well as in charging of secondary batteries (refs. 3 and 4). Romanov reports improved morphology of zinc metal growth from zincate using merely pulsed currents (ref. 5). Two general types of zinc growth morphology are well known (ref. 6): microcrystals (ref. 7, referred to as mossy), which are prevalent at low current densities; and macrocrystals (dendrites, ref. 7; nodules, ref. 8; and/or boulders, ref. 9), which are prevalent at high current densities.

Our approach to the problem was to investigate simultaneously the morphology of the zinc metal deposit and the profile of the ion concentrations involved. In addition, comparisons were made between experiments without pulsing and those with pulse discharging. Our preliminary work shows very little, if any, effect on morphology due to pulsing when comparisons were made on the basis of the same average charging current. However, a correlation was found between zinc growth morphology and ion concentration at the surface. This correlation may eventually lead to an understanding of the mechanism by which, and the degree to which, pulse discharging is effective.

EXPERIMENTAL DETAILS

The Cell

The disassembled cell is shown schematically in figure 1(a); a schematic of the assembled cell is shown in figure 1(b). It consists of two zinc-zincate half-cells and a middle chamber containing a reference zinc-zincate electrode. Each half-cell is separated from the reference chamber by a thin cellulose membrane. (Preliminary work made use of a cell in which the chambers were separated by constrictions rather than membranes.) The presence of additional zinc electrodes (probes) in the half-cell in which the zinc is being electrodeposited (referred to as the cathode chamber) permitted measurement of bulk concentrations in the cathode compartment. The starting electrodes, including the probes, were always new 0.005-centimeter (0.002-in.) thick zinc sheet.

The cell body was made of the polymer polymethylmethacrylate. Its transparency, together with the design of the cell, allowed easy observation via microscope of the zinc growth morphology in situ. Clamping the cell together with bolts was sufficient to prevent leakage.

Cells were run with the electrodes in the horizontal position to minimize gradients parallel to electrode surfaces that would arise from gravitational effects. Most experi-

ments were begun by electrosolution of the cathode for 30 minutes at 6.4 mA/cm^2 and then electrodeposition of zinc back onto the cathode for the same time and at the same current density. This procedure yielded a mossy surface (ref. 10) and the initial catholyte concentration.

Note that, due to low transport of zincate through the cellulose separators (ref. 11), zincate is depleted in the cathode chamber and increased in the anode chamber during a charging experiment. Because of this low transport of zinc through the separators and because the two half-cells were equal in volume, the ion concentrations in the reference chamber remained essentially constant. (Experiments with two electrodes in the reference chamber established that no concentration gradients existed within that chamber.) Also, the fact that only zinc-zincate electrodes were used eliminated the possibility of interference from extraneous ions (e.g., the silver ion).

Electronic Setup

The electronic apparatus is shown schematically in figure 2. The outputs of two signal generators were fed in parallel into a potentiostat. One of the signal generators triggered the other through the variable-delay mechanism of the oscilloscope. The cell current was controlled by having the potentiostat monitor the potential across a standard 10-ohm resistor in series with the cell. Without pulsing, a constant current was obtained. One signal generator created a zero-current interval (0.1-msec duration) every 10 milliseconds. During this zero-current interval the induced polarization potential (ref. 12) was determined across any two electrodes. The second generator added the discharge pulse (inset A, fig. 2) or pulsed current increase (inset B, fig. 2) when desired. Calibration assured us that currents were known to within 1-percent accuracy. The potential between the reference electrode and the various probes (or cathode) was fed into a differential amplifier and then into one channel of the oscilloscope. The potential across the standard resistor was fed into the other channel of the oscilloscope. Readings were estimated to 1 millivolt.

Observation of Zinc Metal Deposit

In situ observations of the zinc deposit during charging experiments were made with a metallographic microscope at 100 magnification. At this magnification, the onset of large crystalline growth (generally referred to as dendritic) was detectable by the first observation of highly reflective crystals. Postexamination of deposits was made via scanning electron microscope (SEM).

Chemicals

The zinc sheet was 5 N pure. The starting potassium hydroxide (KOH) solution was nominally a 45-percent (carbonate free) solution. Several batches of electrolyte were used during the course of this research; each was made by dissolving 50 grams of C. P. zinc oxide in 45-percent KOH solution made up to 500 milliliters. Chemical analyses were obtained on the resultant solutions. The analysis of the batch used for all critical work in this report was 1.21 molar in potassium zincate and 9.00 molar in potassium hydroxide. This agreed well with a calculation based on the composition of the starting material.

RESULTS

Determination of Transition Time

Under constant overvoltage conditions, an initiation time for dendritic growth of zinc between 5 and 100 minutes has been reported (ref. 13). However, it has also been reported (ref. 10) that the transition from moss to dendritic growth for zinc is a function of only current density and temperature; the effect of time was not considered. These data (ref. 10) indicate that at 23° C, above about 22 mA/cm², dendrites (large crystals) would always form.

Our first observation was that during charging at current densities of 25 mA/cm², mossy zinc continued to deposit on an originally mossy substrate. Finally, however, large crystals would start to grow. The time of transition to large crystals was found to depend on current density (fig. 3). The round data points represent constant-charging-current experiments (without zero-current pulsing). The triangular points for pulse discharging are discussed in the following section. (All these data were obtained from the preliminary version of our experimental cell.) The transition time t_t has an approximately logarithmic dependence on current. This type of dependence implies that the amount of moss deposited (before large crystals form) also decreases with increasing current. This was most obvious at high current, for which the amount of mossy deposit was negligibly small.

Error in the measurement of short transition times prevented meaningful determinations at extremely high current densities. Also, the finite cell size prevented meaningful determinations at extremely low current densities, in that during long plating times the entire cathode chamber would become filled with mossy zinc. The same curve (fig. 3) resulted when a predeposit of moss was not used. In contrast, it was generally difficult to plate any moss on a predeposit of large crystals. The same type of dependence

of transition time on current density occurred for cells with separators (fig. 1). The actual transition time, of course, depended on the cathode chamber volume and the type of separation used (separator or constriction).

To substantiate the nature of the deposit, SEM photographs were taken after several experiments. They all exhibited the following (as exemplified in fig. 4): mossy growth at the bottom deposited before the transition, and large crystalline growth at the top deposited after the transition. The large crystals resemble the boulders reported by Bockris, et al. (ref. 9). From our SEM photographs (e.g., fig. 4), we could gain no clue to explain why, at a particular time during plating, the growth morphology should change from mossy to large crystalline deposits. The ratio of metal to void space in the moss was not a function of distance from the collector; from this it was concluded that the plating occurs always on the advancing surface of the mossy growth.

Effect of Pulse Discharging

The charging experiments were repeated using the technique of pulse discharging. Discharging pulses amounting to between 10- and 50-percent discharge were used. Four parameters were varied: charge current i_c , 36 to 80 milliamperes; discharge current i_d , 36 to 450 milliamperes; charge time interval t_c , 0.2 to 700 milliseconds; discharge time interval t_d , 0.1 to 100 milliseconds. Indeed, pulse discharging did increase the time of transition when based on actual charging current i_c . But, from a practical aspect, comparison must be based on the average current \bar{i} , which is a (inverse) measure of the time required to charge a battery:

$$\bar{i} = \frac{i_c t_c - i_d t_d}{t_c + t_d} \quad (1)$$

The results of pulse discharging experiments based on average current are shown in figure 3 as triangular points. There is more scatter among the "pulse discharging" data than among the "unpulsed" data, but no appreciable extension of transition time can be noted. All the pulse discharging data in figure 3 are for charging currents of 62.5 milliamperes with various i_d 's, t_c 's, and t_d 's. Similar data were obtained with charging currents of 36 to 80 milliamperes, but the scatter was greater. Even in six experiments where pulsed "current increase" (fig. 2, inset B) was used, the data points fell on the constant-current curve.

Induced Potential

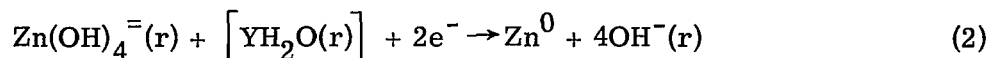
The next step was to monitor various potentials within the cell during a charging experiment. The first potential measured was the one induced across the cathode with respect to an unchanging reference electrode (measured during a zero-current interval). As shown in figure 5, curve A, this value rose immediately from zero to roughly 0.03 volt when charging was begun. During the experiment, it then rose gradually at an ever-increasing rate. For a current of about 30 milliamperes, when the potential reached 0.060 volt (about 0.08 V between cathode and anode), the transition from moss to large crystals occurred. Soon afterward, the potential began to oscillate up to high voltages, roughly 0.5 volt. Somewhat similar oscillations have been previously observed (ref. 14) and explained (ref. 10) by assuming diffusion control and by applying the theory of chronopotentiometry at constant current. We repeated the experiments using pulse discharging; a curve quite similar to curve A in figure 5 resulted when the induced potential was measured right before the discharge pulse. The induced cathode potential at the transition time appeared to decrease somewhat with increasing average current (fig. 6) but seemed to be independent of the parameters we used in pulse discharging.

Induced potentials measured between other electrodes in the cathode chamber and the reference electrode generally showed no rapid initial rise (fig. 5, curve B). Instead, the potential rose slowly at first with an ever-increasing rate. Electrodes near the cathode eventually shorted to the cathode because of the accumulation of electrodeposited zinc. Finally, the potential of unshorted electrodes oscillated in a manner similar to that of the cathode. At least in this case, the oscillations cannot be explained in terms of current flow because neither of the electrodes involved (probe or reference) were passing current. In some way, variations in zincate concentration (which was quite low at this time) were likely to be the cause of this phenomenon.

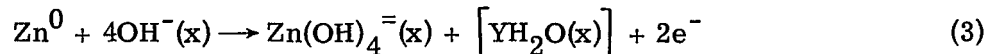
RELATIONSHIP BETWEEN INDUCED POTENTIAL AND CONCENTRATION

To relate the potentials to concentration, the reactions that give rise to the potentials must be established. If $\text{Zn(OH)}_4^{=}$ (ref. 15) is the zincate species involved, the equations are

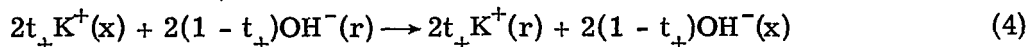
At reference electrode r:



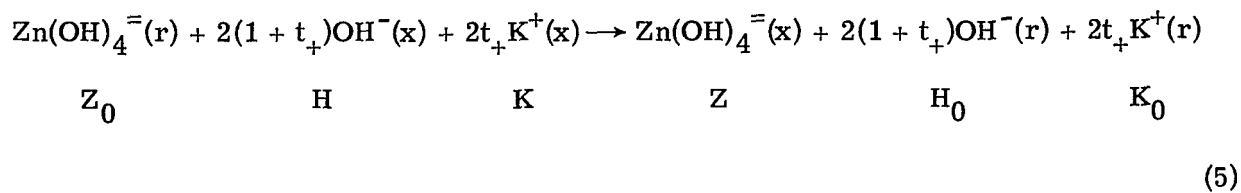
At electrode x:



Due to conductance:



where t_+ is the transference number of the K^+ ion. Water may either be produced (ref. 16) or consumed by the reaction due to differences in hydration between the reactants and the products of the reactions. However, because the molar concentration of water is high (roughly 45 M, calculable from data in ref. 17), the activity of water at both electrodes can be taken to be the same. The overall reaction would thus be



This represents a reaction for a concentration cell with transference. The letter below each formula represents the molar concentration of the respective species. The resultant potential E in volts (reference electrode with respect to the variable electrode so as to result in a positive value) according to the Nernst equation is

$$E = -0.030 \log \frac{\text{Z} \cdot \text{H}_0^{2+2t_+} \cdot \text{K}_0^{2t_+}}{\text{Z}_0 \cdot \text{H}^{2+2t_+} \cdot \text{K}^{2t_+}} \quad (6)$$

when concentrations are used for activities. Defining activity quotients as

$$Q = \frac{\text{Z}}{\text{H}^{2+2t_+} \cdot \text{K}^{2t_+}} \quad (7)$$

yields

$$E = -0.030 \log \frac{Q(x)}{Q(r)} \quad (8)$$

The experimentally measured potentials (if predominantly due to concentration effects) can thereby be converted to values of $Q(x)/Q(r)$. Because $Q(r)$ is constant, $Q(x)$ can be studied as a function of time (and current).

Furthermore, the average value of $Q(x)/Q(r)$ in the cathode chamber can be computed from known parameters as follows:

$$\frac{dZ}{dt} = -\frac{\theta i}{V} \quad (9)$$

$$\frac{dK}{dt} = \frac{2t\theta i}{V} + D(K_0 - K) \quad (10)$$

$$\frac{dH}{dt} = \frac{dK}{dt} - 2 \frac{dZ}{dt} \quad (11)$$

where

$$\theta = \frac{60}{(2 \times 96500)} = 3.11 \times 10^{-4} \text{ M}/(\text{A} \cdot \text{min})$$

i average current, A

t charging time, min

V effective volume of cathode chamber, liters

D diffusion coefficient for KOH through separator, min^{-1}

The diffusion rate of zincate through cellulose is too low (ref. 11) to be included in equation (9). The diffusion coefficient D for KOH through the separator was determined by direct measurement (titrimetrically) in the cell used and found to be 0.014 per minute (a factor of about 40 greater than that for the zincate ion); K^+ was assumed to be the less mobile ion.

To integrate equations (9) to (11) and finally to obtain equations (12) to (15), the following assumptions were made. The volume remains constant; that is, there is no loss or entrainment of electrolyte, and $V = V_0$ (actual volume of the cathode chamber). (With entrainment, $V = V_0(1 - t)/t_e$, where $1/t_e$ is the fraction of electrolyte entrained per minute.) Also, the concentrations of the various species in the reference chamber

were assumed to be constant; the rate of diffusion from the cathode to the reference chamber is equal to the rate of diffusion from the reference to the anode chamber. Thus,

$$Z = Z_0 - \frac{\theta i t}{V_0} \quad (12)$$

$$K = K_0 + \frac{2t_+ \theta i}{V_0 D} (1 - e^{-Dt}) \quad (13)$$

$$H = H_0 + \frac{2\theta i}{V_0} \left[\frac{t_+ (1 - e^{-Dt})}{D} + t \right] \quad (14)$$

Substituting equations (12) to (14) into equation (6) yields

$$\frac{Q(x)}{Q(r)} = \frac{\left(1 - \frac{\theta i t}{V_0 Z_0}\right)}{\left\{1 + \frac{2\theta i}{V_0 H_0} \left[\frac{t_+ (1 - e^{-Dt})}{D} + t\right]\right\}^{2+2t_+} \left[1 + \frac{2t_+ \theta i}{V_0 D K_0} (1 + e^{-Dt})\right]^{2t_+}} \quad (15)$$

Inspection of equations (12) to (15) shows that during charging, the values of K and H increase with time while Z decreases.

From equation (15), the average value of $Q(x)/Q(r)$ in the cathode chamber at time t can be computed from known parameters (average current, volume of cathode chamber, starting concentrations, time, and diffusion coefficient) and the transference number t_+ , which may be estimated. The solid and short-dashed curves in figure 7 show graphically the predicted dependence of $Q(x)/Q(r)$ on time (for $i = 30$ mA; $V = 0.00109$ liter; $K_0 = 11.42$ m/liter; $H_0 = 9.00$ M/liter; $Z = 1.21$ M/liter; and $D = 0.014$ /min). The difference between the curves is caused by assuming $t_+ = 0.5$ for the solid curve and $t_+ = 0.4$ for the short-dashed curve; thus, equation (15) is not very sensitive to t_+ . For simplicity, we have used $t_+ = 0.5$ for subsequent calculations. The long-dashed line in figure 7 represents the use of $D = 0.00014$ per minute. Thus, equation (15) is, likewise, not very sensitive to the value of D and so the following equation approximates equation (15):

$$\frac{Q(x)}{Q(r)} = \frac{\left(1 - \frac{\theta i t}{V_0 Z_0}\right)}{\left(1 + \frac{3\theta i t}{V_0 H_0}\right)^3 \left(1 + \frac{\theta i t}{V_0 K_0}\right)} \quad (16)$$

However, equations (15) and (16) do not give $Q(c)/Q(r)$ for the surface of the cathode collector because concentration gradients can exist in the catholyte. Even if the catholyte is well mixed by convection, a gradient should still exist across the boundary layer and the adsorbed species will not be in equilibrium with the bulk concentrations. This gradient should be proportional to the flow by Fick's law, and the flow should be proportional to the current density i/a (where a = area). In turn, the difference Δ between the bulk concentration and the activity of a species on the surface (expressed in concentration units for simplicity even though such units cannot be applied directly to the activity of adsorbed species) is proportional to the product of the gradient and the boundary layer thickness y . With the assumption that y and a are constants, they can be incorporated into the proportionality constant γ , so that

$$Z(c) - Z(x) = \Delta_1 = \gamma_1 i \quad (17)$$

for the zincate concentration difference. Similar equations can be written for the other concentration differences. In practice, there may be two (or more) regions of gradient, one across the boundary layer and one across the surface interface; Δ would encompass both gradients.

Moreover, when considering the cathode electrode, we must recognize that its surface is mossy (or crystalline) while the reference electrode is a smooth foil. Thus, an activity correction, a factor M , that corrects for the relative stress in the two collectors should be included in the equation. Over and above this, the chemical rate-determining step may introduce a nonequilibrium concentration factor into the equation (eqs. (A31) and (A32)). However, this factor is probably negligible and is not necessary for interpreting the data. Using equations (12) and (17), one may write

$$Z(c) = Z_0 \left(1 - \frac{\theta i t}{V_0 Z_0} - \frac{\gamma_1 i}{Z_0}\right) \quad (18)$$

Similar equations may be written for $H(c)$ and $K(c)$. Using such equations yields

$$e^{-2EF/RT} = \frac{Q(c)}{Q(r)} = \frac{Z \cdot H_0^3 \cdot K_0}{M \cdot Z_0 \cdot H^3 \cdot K} = \frac{\left(1 - \frac{\theta i t}{V_0 Z_0} - \frac{\gamma_1 i}{Z_0}\right)}{M \left(1 + \frac{3\theta i t}{V_0 H_0} + \frac{\gamma_2 i}{H_0}\right)^3 \left(1 + \frac{\theta i t}{V_0 K_0} + \frac{\gamma_3 i}{K_0}\right)} \quad (19)$$

Equation (19) should only be applied when the concentrations in the bulk of the cathode chambers are somewhat uniform. When the zincate concentration ($Z(c)$ in eq. (18)) equals zero, $Q(c)/Q(r)$ must equal zero, so that t_i (time intercept) is given by the following equation:

$$t_i = \frac{Z_0 V_0}{\theta i} - \frac{\gamma_1 V_0}{\theta} \quad (20)$$

A plot of t_i (i.e., t at $Q(c)/Q(r) = 0$) versus $1/i$ can uniquely determine γ_1 . In contrast, evaluation of equation (19) at $t = 0$ yields

$$\left(\frac{Q(r)}{Q(c)}\right)_{t=0} \left(1 - \frac{\gamma_1 i}{Z_0}\right) = M \left(1 + \frac{\gamma_2 i}{H_0}\right)^3 \left(1 + \frac{\gamma_3 i}{K_0}\right) \quad (21)$$

By expansion, with the assumption that terms in i^2 are not important and γ_2 and γ_3 may be of comparable magnitude, equation (21) becomes

$$\sqrt[4]{\left(\frac{Q(r)}{Q(c)}\right)_{t=0} \left(1 - \frac{\gamma_1 i}{Z_0}\right)} = \sqrt[4]{M} \left[1 + \frac{\gamma_2 i}{4} \left(\frac{3}{H_0} + \frac{1}{K_0}\right)\right] \quad (22)$$

Thus, a plot of the left side of equation (22) (if γ_1 is known) versus i allows M to be calculated from the slope and γ_2 to be approximated from the intercept.

Also, the value of $Z(c)$ on the surface can be calculated for any time from the equation

$$Z(c) = \frac{\theta i}{V_0} (t_i - t) \quad (23)$$

which was derived by rearrangement and combination of equations (18) and (20).

COMPARISON OF EXPERIMENTAL DATA WITH PREDICTED VALUES

Cathode Chamber

Values of $Q(x)/Q(r)$ were calculated from experimental values of E for probes (electrodes) in the cathode chamber via equation (8); representative data are plotted as a function of time in figure 8. (The values of $Q(c)/Q(r)$ are also plotted.) Scatter, though present, does not obscure the fact that $Q(x)/Q(r)$ decreases (not quite linearly) with time and finally becomes essentially zero. The solid curve in figure 8 is that predicted for the average value of $Q(x)/Q(r)$ via equation (15).

The experimental values (fig. 8) for three different electrodes approximate the predicted curve. However, a slight gradient is indicated by the experimental values with the concentration nearest the separator being the greatest. The complete absence of a gradient would denote perfect mixing; the fact that the gradient is slight indicates the chamber is fairly well mixed, probably by self-induced convective flow. Similar agreement also exists between experimental $Q(x)/Q(r)$ values and predicted ones for the other currents used.

The fact that the time intercept for the experimental data (about 140 min from fig. 8) agrees with the predicted intercept (141 min from eq. (15)) shows that essentially all the zincate present in the cathode chamber at the beginning of the run is reduced during charging to metallic zinc. Thus, entrainment is negligible and any zincate remaining behind the advancing metal surface is eventually reduced to zinc metal. Moreover, the agreement between the experimental and predicted curves is evidence that the reactions proposed (eqs. (2) to (5)) are suitable for describing the process actually occurring as well as for explaining the cause of the measured, induced electrochemical potential.

The existence of convective flow in our cathode chamber may explain why pulse discharging was not effective under our experimental conditions. It is claimed that the beneficial effects of pulse discharging are due to its effect on the diffusion profile in the bulk (ref. 2); this assumes the absence of convective flow. Indeed, the morphology of zinc deposits has been shown to be a function of electrolyte flow (ref. 18). In contrast, in batteries, porous materials such as asbestos in contact with the electrode may inhibit convective flow.

Cathode Surface

Figure 8 (solid points) also shows $Q(c)/Q(r)$ as a function of time. The much smaller magnitude as compared with $Q(x)/Q(r)$ at corresponding times implies either relatively large concentration differences across the boundary layer or a large value for

M. To evaluate the difference in zincate concentration across the boundary layer (or more correctly γ_1), $t_{(Q(c)/Q(r)=0)}$ (i.e., t_i for various i 's) was plotted against $1/i$ (fig. 9). This plot yields a slope of 4.28 ampere-minutes, in good agreement with the 4.25 ampere-minutes predicted from equation (20). From the intercept, $\gamma_1 = 13.5$ (M/liter)/A; in terms of current density, the value is 11 (M/liter)/(A/cm²).

In figure 10, the zincate concentration was schematically plotted against the distance from the cathode collector, making use of our knowledge that the bulk of the catholyte is well mixed and that a concentration difference exists between the bulk concentration and the concentration at the cathode collector surface. Plots are given for three different current densities: 0.010, 0.020, and 0.040 A/cm². Plots are also given for two different bulk zincate concentrations: 1.21 molar (initial value) and 0.45 molar (63-percent depletion of zincate). These graphs are based on the value of γ_1 that was determined by assuming that the boundary layer thickness was independent of current and zincate concentration.

Figure 10 illustrates, that at a given current density, the concentration difference between the bulk and the collector surface remains constant with time while the bulk concentration changes. It also illustrates that this difference increases with increasing current.

The curve for 0.040 A/cm² and 63-percent depletion shows a zincate concentration at the surface of about zero. In that the concentration cannot drop below zero, further deposition requires that the current density be reduced or hydrogen gas will be evolved.

Next, the values of

$$\left(\sqrt[4]{\frac{Q(r)}{Q(c)} \left(\frac{1 - \gamma_1 i}{Z_0} \right)} \right)_{t=0}$$

were plotted against i in figure 11 according to equation (22). Special experiments were performed to obtain values at low currents. The plot yields a value of M of about 2, equivalent to a 9-millivolt difference between the moss (cathode) collector and the reference electrode (sheet zinc). The slope of the curve in figure 11 yields (according to eq. (22)) an approximate value of 20 (M/liter)/A for γ_2 ; in terms of current density, 16 (M/liter)/(A/cm²). In that the diffusion rate of the hydroxide ion should be large with respect to that for the zincate ion, one would expect γ_2 to be small with respect to γ_1 (the γ 's being essentially the reciprocals of the diffusion coefficients). To explain the large value for γ_2 , we propose it arises from a slow desorption of the hydroxide ion.

Equation (23) can be used to calculate Z_t the surface concentration of zincate at the transition time. This concentration is shown as a function of current in figure 12. The scatter is large, but the data indicate that Z_t is not constant at the time of transi-

tion from moss to large crystalline growth but increases with increasing i . Actually, Z_t varies by an order of magnitude in the range of currents that were investigated.

INTERPRETATION OF THE INDUCED VOLTAGE AT TRANSITION

The question now arises, "Why does the morphology convert from moss to dendritic at some point in time?" Our proposed answer is that the type of deposit should depend on the concentration of some species at the surface. The most likely ones are those involved in the actual deposition (eq. (A4)): $ZnOH$ and OH^- .



Unlikely candidates are K^+ , which is not involved in any chemical reaction, and $Zn(OH)_4^{2-}$, which has been shown to vary widely with current at the transition.

Rearranging equation (19) and using equation (23) yield

$$\ln i(t_i - t_t) = -\left(\frac{2F}{RT}\right)E_t + \ln\left(\frac{H_t}{H_0}\right)^3 \left(\frac{K_t}{K_0}\right) \frac{Z_0 V_0 M}{\theta} \quad (25)$$

A plot of $\ln i(t_i - t_t)$ versus E_t is shown in figure 13. The straight line that is drawn to approximate the points has a slope close to $-2F/RT$, in accord with equation (25). The fact that the data points appear to fall on this line would indicate that $(H_t/H_0)^3 \cdot (K_t/K_0)$ is a constant at the transition time regardless of current. From this finding, we postulate that it may be the hydroxide concentration at the surface H that determines the morphology of zinc growth. From the intercept ($E_t = 0$) in figure 13, $(H_t/H_0)^3 \cdot (K_t/K_0)$ can be calculated to be 2.5. Evaluation of H_t (H at t_t) from the present data can only be approximate because precise values of γ_2 and γ_3 are not known. Because K^+ is not involved in any chemical reaction, it is reasonable to assume that $K_t/K_0 = 1$ (or at least is closer to 1 than H_t/H_0). Thus, $H_t/H_0 = \sqrt[3]{2.5}$, or 1.35, and H_t would be 12 molar. Below this value, mossy zinc forms; above this value, crystalline zinc forms.

Lewis Research Center

National Aeronautics and Space Administration,

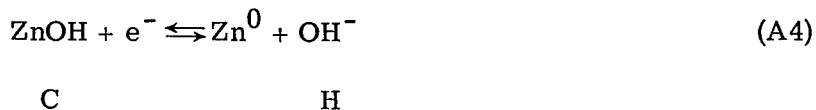
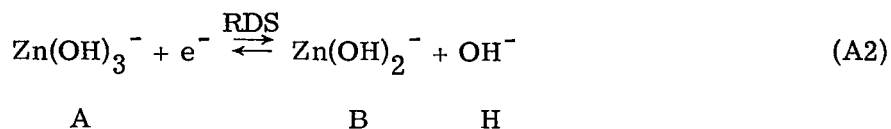
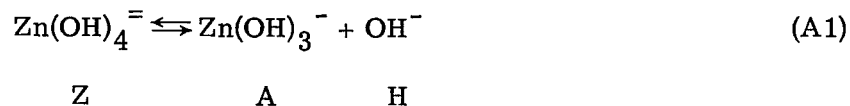
Cleveland, Ohio, April 18, 1977,

506-16.

APPENDIX A

EFFECT OF CHEMICAL NONEQUILIBRIUM

In this appendix, we determine how the lack of chemical equilibrium might affect the measured induced potential. The reaction mechanism as supported by the work of Bockris, et al. (ref. 19) is



Under each chemical formula is the letter that represents its molar concentration (or more correctly, its surface activity). According to the Butler-Volmer equation (ref. 20), the current (during zero pulse) is

$$0 = k_2 A e^{\frac{-\beta_2 \epsilon F}{RT}} - l_2 B H e^{\frac{(1-\beta_2) \epsilon F}{RT}} + k_4 C e^{\frac{-\beta_4 \epsilon F}{RT}} - l_4 M H e^{\frac{(1-\beta_4) \epsilon F}{RT}} \quad (\text{A5})$$

where

ϵ half-cell potential

F Faraday constant

R gas constant

T temperature, K

k, l rate constants
 β 's symmetry factors
 M activity of zinc collector

With rearrangement of equation (A5),

$$e^{\epsilon F/RT} = \frac{k_2 A + k_4 C e^{(\beta_2 - \beta_4) \epsilon F/RT}}{l_2 B + l_4 M e^{(\beta_2 - \beta_4) \epsilon F/RT}} \quad (A6)$$

In that equations (A1) and (A3) are in equilibrium, A and C can be expressed in terms of Z, B, and H as

$$e^{\epsilon F/RT} = \left[\frac{\frac{k_1 k_2}{l_1} Z + \frac{k_4 k_3 B}{l_3} e^{(\beta_2 - \beta_4) \epsilon F/RT}}{l_2 B + l_4 M e^{(\beta_2 - \beta_4) \epsilon F/RT}} \right] \frac{1}{H^2} \quad (A7)$$

Consider now that under certain circumstances B may not be in equilibrium; thus, an equation may be written describing B_e (B at equilibrium),

$$B_e = \sqrt{\frac{Z M k_1 k_2 l_3 l_4}{l_1 l_2 k_3 k_4}} \quad (A8)$$

Combining equations (A7) and (A8) gives

$$e^{\epsilon F/RT} = \frac{1}{H^2} \left[\frac{\frac{k_1 k_2 Z}{l_1} + \frac{k_3 k_4}{l_3} \left(\frac{B}{B_e} \right) \sqrt{\frac{Z M k_1 k_2 l_3 l_4}{l_1 l_2 k_3 k_4}} e^{(\beta_2 - \beta_4) \epsilon F/RT}}{l_2 \left(\frac{B}{B_e} \right) \sqrt{\frac{Z M k_1 k_2 l_3 l_4}{l_1 l_2 k_3 k_4}} + l_4 M e^{(\beta_2 - \beta_4) \epsilon F/RT}} \right] \quad (A9)$$

Rearrangement yields

$$e^{\epsilon F/RT} = \left(\frac{B}{B_e} \right) \frac{\sqrt{\frac{Zk_1k_2k_3k_4}{Ml_1l_2l_3l_4}}}{H^2} \frac{\frac{B_e}{B} \sqrt{\frac{k_1k_2l_3l_4}{l_1l_2k_3k_4}} e^{(\beta_2 - \beta_4)\epsilon F/RT} + 1}{\frac{B}{B_e} \sqrt{\frac{k_1k_2l_3l_4}{l_1l_2k_3k_4}} e^{(\beta_2 - \beta_4)\epsilon F/RT} + 1} \quad (\text{A10})$$

Because equation (A2) is rate determining, $l_2 \cdot k_2 \ll l_4 \cdot k_4$. Equation (A10) can thus be simplified as

$$e^{\epsilon F/RT} = \frac{\sqrt{\frac{Zk_1k_2k_3k_4}{Ml_1l_2l_3l_4}} \left(\frac{B}{B_e} \right)}{H^2} \quad (\text{A11})$$

The potential of the reference chamber ϵ_0 is similarly given, but $B = B_e$ and $M = 1$.

$$e^{\epsilon_0 F/RT} = \frac{\sqrt{\frac{Zk_1k_2k_3k_4}{l_1l_2l_3l_4}}}{H^2} \quad (\text{A12})$$

The potential measured would be given by the equation

$$E = \epsilon_0 + \epsilon_j - \epsilon \quad (\text{A13})$$

where ϵ_j is the junction potential and

$$e^{\epsilon_j F/RT} = \left(\frac{K}{K_0} \right)^{t_+} \left(\frac{H}{H_0} \right)^{t_+ - 1} \quad (\text{A14})$$

Combining equations (A11) to (A14) yields

$$e^{-2EF/RT} = \frac{Z}{MZ_0} \left(\frac{H_0}{H} \right)^{2+2t_+} \left(\frac{K_0}{K} \right)^{2t_+} \left(\frac{B}{B_e} \right)^2 \quad (\text{A15})$$

Thus, nonequilibrium introduces the factor $(B/B_e)^2$ into the Nernst equation. Taking equation (A15) a step further by using Z from equation (A8) and B_0 as the value of B in the reference chamber yields

$$e^{-EF/RT} = \frac{B}{MB_0} \left(\frac{H_0}{H} \right)^{1+t_+} \left(\frac{K_0}{K} \right)^{t_+} \quad (\text{A16})$$

Equation (A16) is the Nernst equation expected for equations (A3) and (A4) alone. Moreover, returning to equation (A10) and assuming (contrary to fact) that equation (A4) is rate controlling yield

$$e^{\epsilon F/RT} = \frac{\sqrt{\frac{Zk_1k_2k_3k_4}{Ml_1l_2l_3l_4}} \left(\frac{B_e}{B} \right)}{H^2} \quad (\text{A17})$$

instead of equation (A11),

$$e^{-2EF/RT} = \frac{Z}{MZ_0} \left(\frac{H_0}{H} \right)^{2+2t_+} \left(\frac{K_0}{K} \right)^{2t_+} \left(\frac{B_e}{B} \right)^2 \quad (\text{A18})$$

instead of equation (A15), and thus

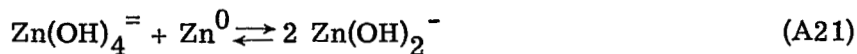
$$e^{-EF/RT} = \left(\frac{Z}{Z_0} \right) \left(\frac{B_0}{B} \right) \left(\frac{H_0}{H} \right)^{1+t_+} \left(\frac{K_0}{K} \right)^{t_+} \quad (\text{A19})$$

instead of equation (A16). Equation (A19) is the Nernst equation expected for equations (A1) and (A2). Thus, it appears that when chemical equilibrium is not present, the measured induced potential is characteristic of the non-rate-controlling step.

The lack of chemical equilibrium in our experiments could, of course, be produced during the current pulse. The Butler-Volmer equation (during the passage of current) can be given in terms of the rate-determining step (eq. (A2))

$$i = Ak_2 e^{-\phi F \beta_2 / RT} - BHl_2 e^{\phi F (1-\beta_2) / RT} + i_4 \quad (\text{A20})$$

where ϕ is the potential and i_4 (current due to eq. (A4)) would ordinarily be $i/2$ for a two-electron process. However, we may write an equation in addition to those involved in the reaction mechanics,



Such an equation would result in i_4 not equaling $i/2$. To correct for this, consider the change of B with time,

$$\frac{dB}{dt} = Ak_2 e^{-\beta_2 \phi F/RT} - BHe^{(1-\beta_2) \phi F/RT} - i_4 + k_5 ZM - l_5 B^2 = 0 \quad (\text{A22})$$

Because of steady-state conditions, $dB/dt = 0$. The symbols k_5 and l_5 are rate constants for equation (A21) and

$$k_5 ZM = l_5 B^2 \quad (\text{A23})$$

Combining equations (A20) and (A22) yields

$$i = 2 \left[Ak_2 e^{-\beta_2 \phi F/RT} - BHe^{(1-\beta_2) \phi F/RT} \right] + k_5 ZM - l_5 B^2 \quad (\text{A24})$$

Because equations (A1), (A3), and (A4) are in equilibrium,

$$k_1 Z = l_1 AH \quad (\text{A25})$$

$$k_3 B = l_3 CH \quad (\text{A26})$$

$$k_4 C = l_4 MHe^{\phi F/RT} \quad (\text{A27})$$

Substituting equations (A25) to (A27) into equation (A24) gives

$$i = 2 \left[\left(\frac{k_1 k_2 Z}{l_1 H} \right) \left(\frac{k_3 k_4 B}{l_3 l_4 M H^2} \right)^{-\beta_2} - BHe^{(1-\beta_2) \phi F/RT} \right] + k_5 ZM - l_5 B^2 \quad (\text{A28})$$

Using equations (A8) and (A23) yields

$$i = \frac{2H^{(2\beta_2-1)}Z^{(1-\beta_2/2)}\left(\frac{l_1l_2l_3l_4M}{k_1k_2k_3k_4}\right)^{\beta_2/2}}{\left(\frac{B}{B_e}\right)^{\beta_2}} \frac{k_1k_2}{l_1} \left[1 - \left(\frac{B}{B_e}\right)^2\right] + \left[1 - \left(\frac{B}{B_e}\right)^2\right] k_5 Z M \quad (\text{A29})$$

When B is only slightly displaced from equilibrium, equation (A29) can be simplified as

$$1 - \lambda i = \left(\frac{B}{B_e}\right)^2 \quad (\text{A30})$$

where λ is a combination of the constants as well as Z, H, and M. Combining equation (A30) with equation (A15) gives

$$e^{-2EF/RT} = \frac{Z}{MZ_0} \left(\frac{H_0}{H}\right)^{2+2t_+} \left(\frac{K_0}{K}\right)^{2t_+} (1 - \lambda i) \quad (\text{A31})$$

Because Z, H, and K also possess polarizations due to current, the value of E can be expressed at $t = 0$ as

$$e^{-2EF/RT} = \frac{\left(1 - \frac{\gamma_1 i}{Z_0}\right) (1 - \lambda i)}{M \left(1 + \frac{\gamma_2 i}{H_0}\right)^3 \left(1 + \frac{\gamma_3 i}{K_0}\right)} \quad (\text{A32})$$

From our experimental data, γ_1 can be calculated via equation (19) and M via extrapolation of $e^{-2EF/RT}$ to zero current. However, γ_2 , γ_3 , and λ cannot be uniquely determined. In this report, we have assumed that λ is negligible and that γ_3 is comparable to γ_2 , in order to obtain an approximate value for γ_2 . Our personal belief is that λ is truly negligible; but we must acknowledge that it is possible for λ to affect the polarization potential E (eq. (A32)).

APPENDIX B

SYMBOLS

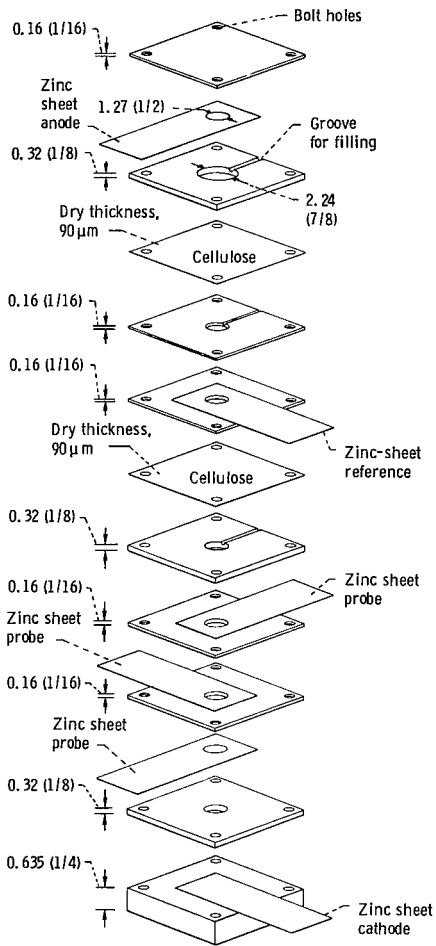
A	Zn(OH)_3^- molar concentration
a	cross-sectional area of cell
B	Zn(OH)_2^- molar concentration
B_e	equilibrium Zn(OH)_2^- molar concentration
B_0	Zn(OH)_2^- molar concentration in reference chamber
C	Zn(OH) molar concentration
(c)	cathode surface
D	diffusion coefficient of KOH through separator
E	induced potential during zero-current interval
E_t	induced potential during zero-current interval at transition time
F	Faraday constant
H	OH^- molar concentration
H_0	OH^- molar concentration in reference chamber
H_t	OH^- molar concentration at transition time
i	current
\bar{i}	average current
i_c	charge current
i_d	discharge current
i_4	current due to reaction (eq. (A4))
K	K^+ molar concentration
K_0	K^+ molar concentration in reference chamber
K_t	K^+ molar concentration at transition time
k_1, k_2, k_3, k_4, k_5	forward rate constants for eqs. (A1), (A2), (A3), (A4), and (A21), respectively
l_1, l_2, l_3, l_4, l_5	reverse rate constants for eqs. (A1), (A2), (A3), (A4), and (A21), respectively
M	apparent activity of mossy zinc

Q	activity quotient
R	gas constant
(r)	reference chamber
T	absolute temperature
t	time
t_c	charge time interval
t_d	discharge time interval
t_e	time required for cathode chamber to fill with moss
t_i	time when $Q(c)/Q(r) = 0$
t_t	moss-to-large-crystal transition time
t_+	transference number of K^+ ion
V	catholyte volume
V_0	volume of catholyte chamber
(x)	cathode chamber
y	boundary layer thickness
Z	$Zn(OH)_4^-$ molar concentration
Z_0	$Zn(OH)_4^-$ molar concentration in reference chamber
Z_t	$Zn(OH)_4^-$ molar concentration at cathode collector at transition time
β_2, β_4	symmetry factors for eqs. (A2) and (A4), respectively
$\gamma_1, \gamma_2, \gamma_3$	proportionality constants for dependence of concentration differences across boundary layer on current, for Z, H, and K, respectively
Δ	concentration difference between cathode surface and bulk
Δ_1	zincate concentration difference between cathode surface and bulk
ϵ	potential of working half-cell
ϵ_j	junction potential
ϵ_0	potential of reference half-cell
θ	$60/2F$
λ	proportionality constant relating B and B_e
ϕ	potential applied across working half-cell

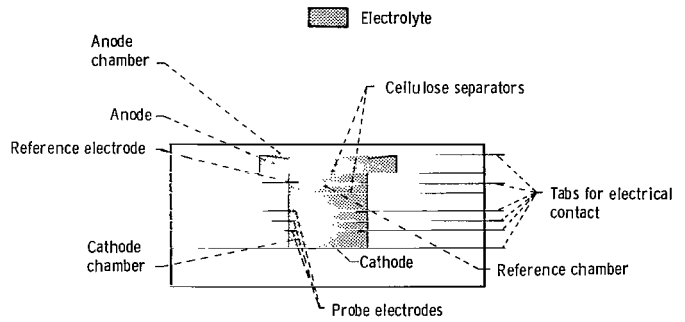
REFERENCES

1. Sparks, R. H.: Rapid Charging Batteries for Electric Propulsion Systems. Automotive Engineering Conference. SAE Paper 720109, Jan. 1972.
2. Despic, A. R.; and Popov, K. I.: The Effect of Pulsating Potential on the Morphology of Metal Deposits Obtained by Mass-Transport Controlled Electrodeposition. *J. Appl. Electrochem.*, vol. 1, 1971, pp. 275-278.
3. Wales, Charles P.: Charging the Silver Oxide Electrode with Periodically Varying Current. *J. Electrochem. Soc.*, vol. 115, no. 10, Oct. 1968, pp. 985-990.
4. Arouette, S.; Blurton, K. F.; and Oswin, H. G.: Controlled Current Deposition of Zinc from Alkaline Solution. *J. Electrochem. Soc.*, vol. 116, no. 2, Feb. 1969, pp. 166-169.
5. Romanov, U. V.: Possibility of Decreasing Growth of Dendritic Zinc in Nickel-Zinc and Silver-Zinc Batteries. *Zhur. Priklode Khim*, vol. 34, 1961, pp. 2692-2699.
6. Oswin, H. G.; and Blurton, K. F.: The Morphology of Zinc Electrodeposited from Alkaline Electrolyte. *Zinc-Silver Oxide Batteries*, Arthur Fleischer and John J. Lander, eds., John Wiley & Sons, Inc., 1971, pp. 63-85.
7. Stachurski, Z. O. J.: Study to Investigate and Improve the Zinc Electrode for Spacecraft Electrochemical Cells. (Yardney Electric Co., NAS5-10231) NASA CR-89299, 1967.
8. Bozek, John M.: Structure and Function of an Inorganic-Organic Separator for Electrochemical Cells - Preliminary Study. NASA TM X-3080, 1974.
9. Bockris, J. O'M.; Nagy, Z.; and Drazic, D.: On the Morphology of Zinc Electrodeposition from Alkaline Solution. *J. Electrochem. Soc.*, vol. 120, no. 1, Jan. 1973, pp. 30-41.
10. Oxley, J. E.; and Fleischmann, C. N.: The Improvement of Zinc Electrodes for Electrochemical Cells. (Leesona Corp.; NAS5-9591) NASA CR-70724, 1965.
11. Phillipp, Warren H.; and May, Charles E.: Functioning of Inorganic/Organic Battery Separators in Silver-Zinc Cells. NASA TM X-3357, 1976.
12. Yeager, Ernst; and Salkind, Alvin J.: *Techniques of Electrochemistry*. Vol. 1, Wiley-Interscience, 1972, p. 152.
13. Diggle, J. W.; Despic, A. R.; and Bockris, J. O'M.: The Mechanism of the Dendritic Electrocrystallization of Zinc. *J. Electrochem. Soc.*, vol. 116, no. 11, Nov. 1969, pp. 1503-1514.

14. Oxley, J. E.; and Fleischmann, C. W.: Improvement of Zinc Electrodes for Electrochemical Cells. (Leesona Corp.; NAS5-9591) NASA CR-68646, 1965.
15. Briggs, A. Gordon; Hampson, Noel A.; and Marshall, Alan: Concentrated Potassium Zincate Solutions Studied Using Laser Raman Spectroscopy and Potentiometry. J. Chem. Soc. (Far. Trans. II), vol. 70, pt. 11, 1974, pp. 1978-1990.
16. Despic, A. R.; Jovanovic, D. J.; and Rakic, T.: Kinetics and Mechanism of Deposition of Zinc from Zincate in Concentrated Alkali Hydroxide Solutions. Electrochimica Acta, vol. 21, no. 1, Jan. 1976, pp. 63-77.
17. Weast, R. C., ed.: Handbook of Chemistry and Physics. 52nd ed., 1971-1972, p. 205.
18. Naybour, R. D.: The Effect of Electrolyte Flow on the Morphology of Zinc Electrodeposited from Aqueous Alkaline Solution Containing Zincate Ions, J. Electrochem. Soc., vol. 116, no. 4, Apr. 1969, pp. 520-524.
19. Bockris, J. O'M.; Nagy, Z.; and Damjanovic, A.: On the Deposition and Dissolution of Zinc in Alkaline Solutions. J. Electrochem. Soc., vol. 119, no. 3, Mar. 1972, pp. 285-295.
20. Bockris, J. O'M.; and Reddy, A. K. N.: Modern Electrochemistry. Vol. 2, ch. 8, Plenum Press, 1970, pp. 845-990.

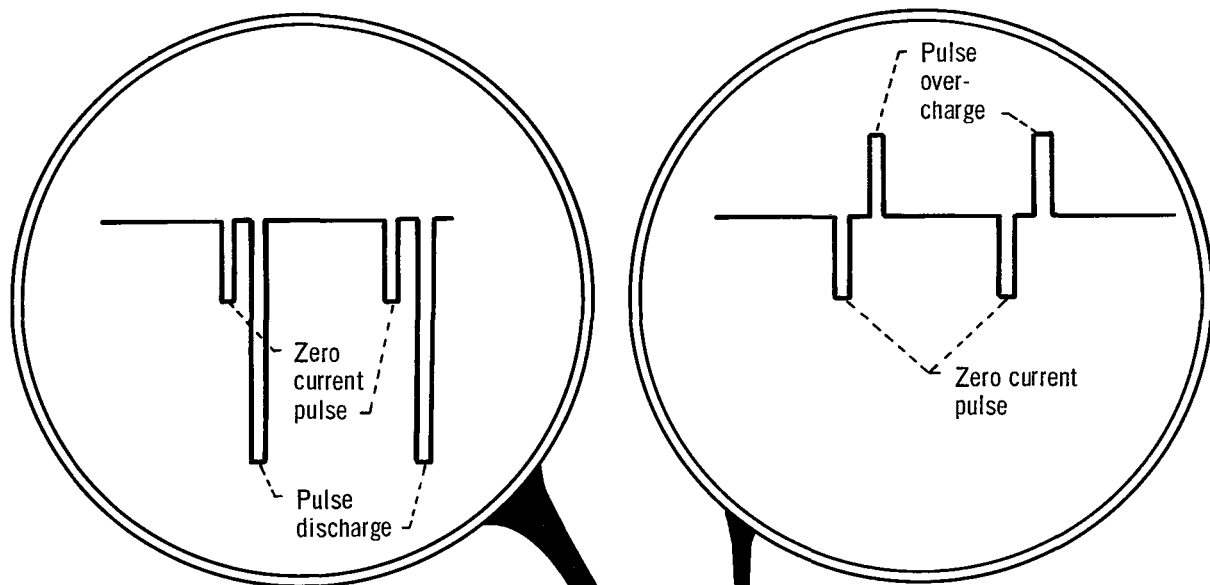


(a) Disassembled cell. (Dimensions not otherwise specified are in cm (in.); material not specified is polymethylmethacrylate; central holes without specified diameters are 1.27 cm in diameter.)



(b) Assembled cell.

Figure 1. - Schematics of cell.



Inset A

Inset B

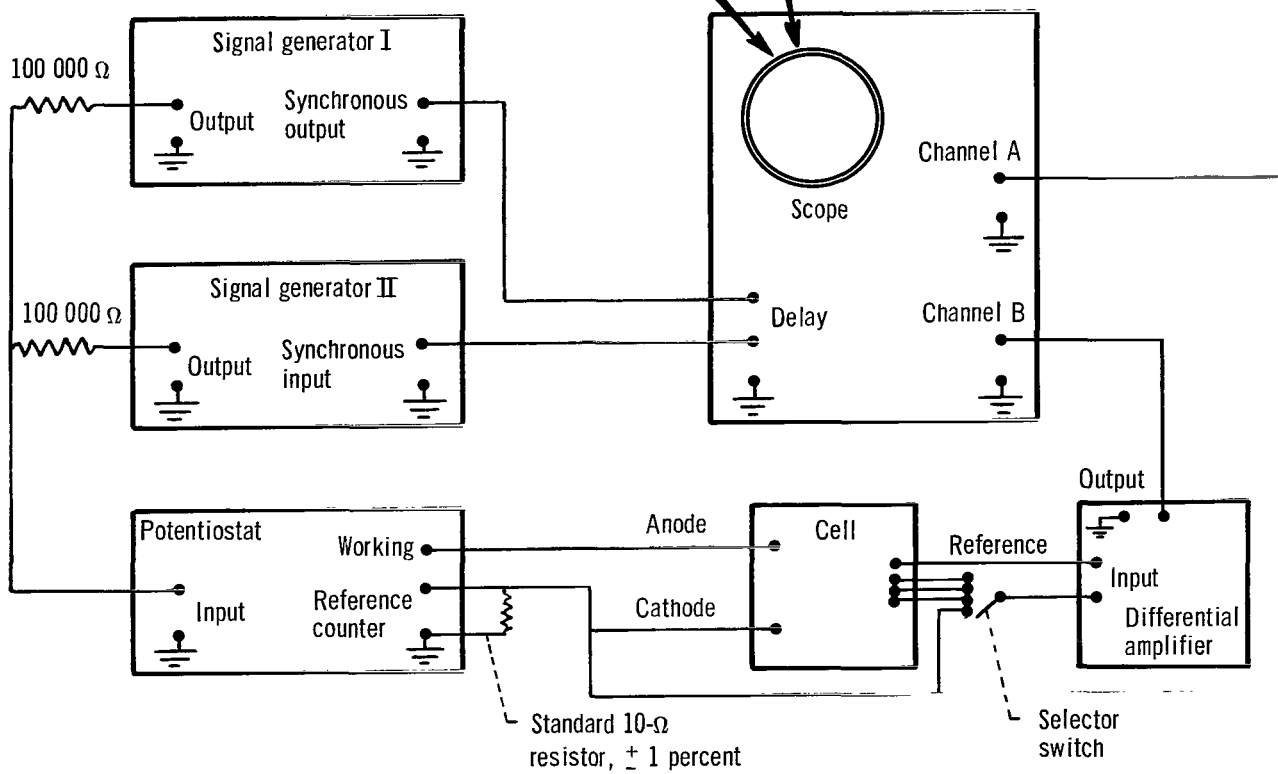


Figure 2. - Schematic of electronic setup.

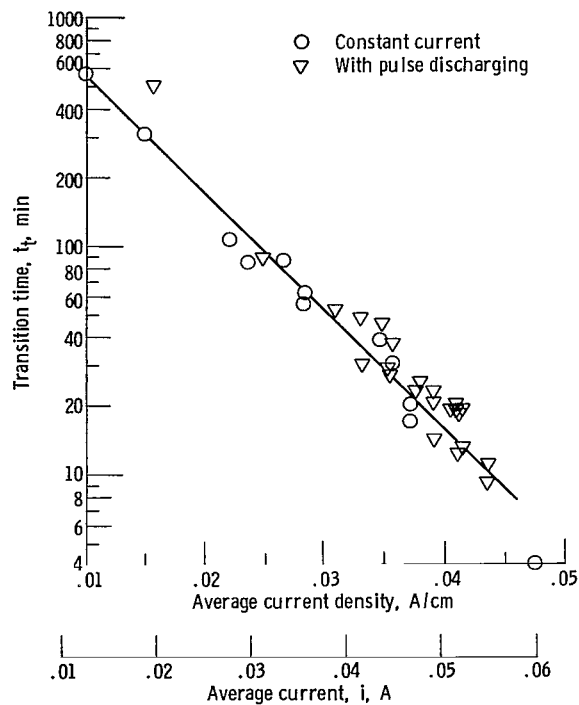


Figure 3. - Dependence of morphology on current density and time. Cross-sectional area of cell, a , 1.26 cm^2 ; volume of catholyte chamber, V_0 , 0.79 cm^3 .

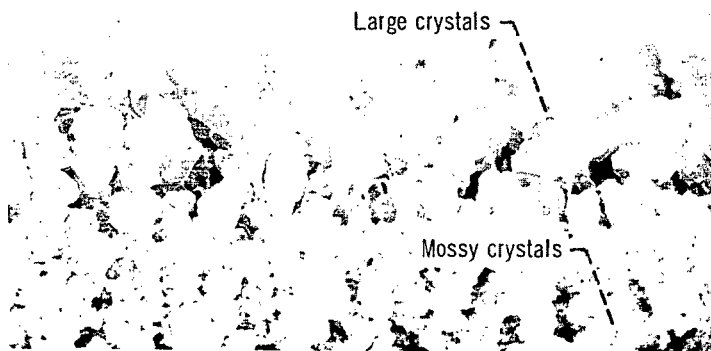


Figure 4. - Scanning electron micrograph of cross section of zinc metal growth. $\times 100$.

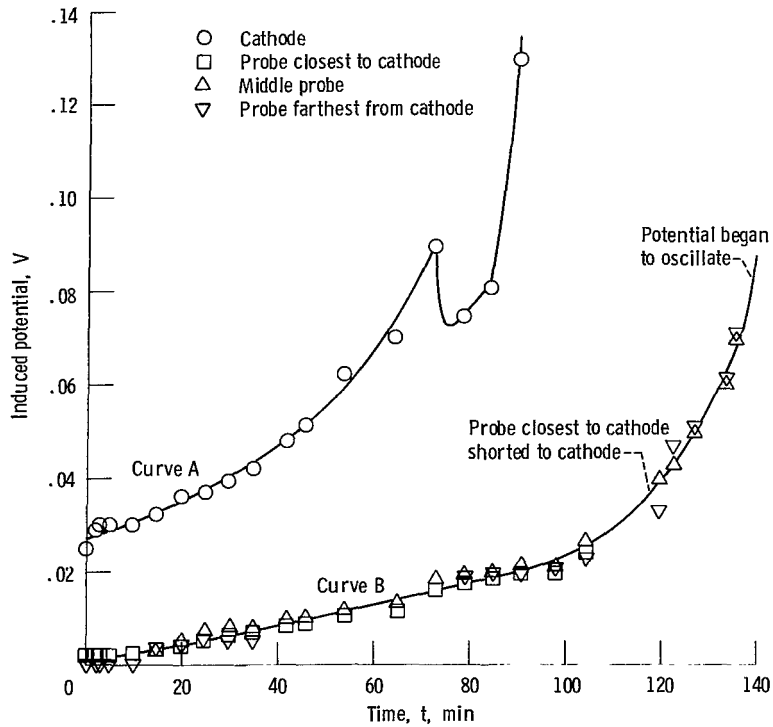


Figure 5. - Induced potentials in cathode chamber. Current, i , 0.030 A.

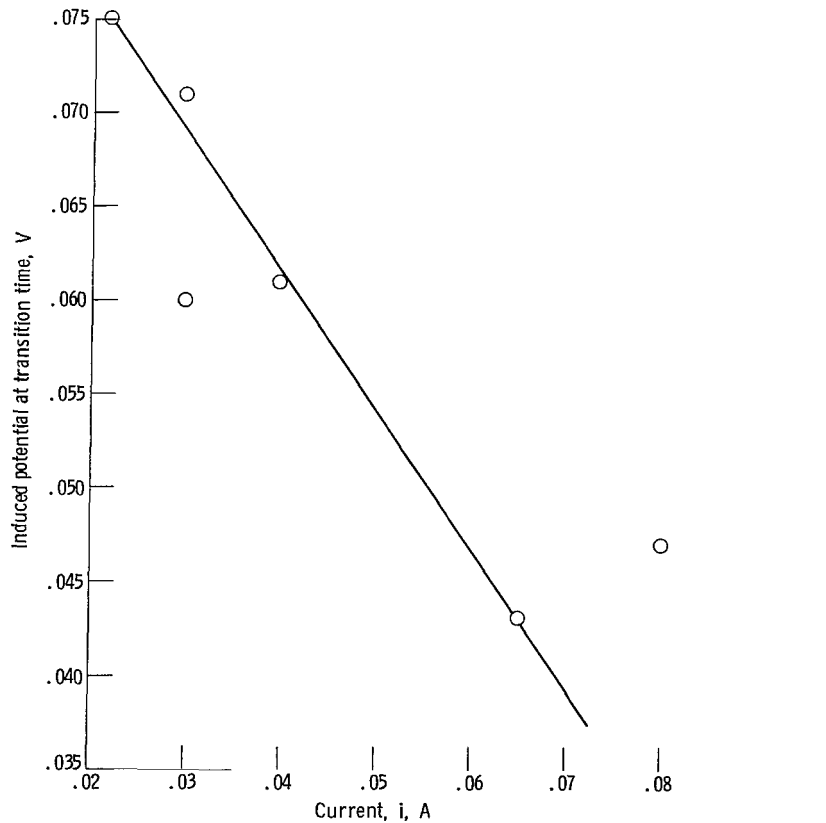


Figure 6. - Induced potential at transition time.

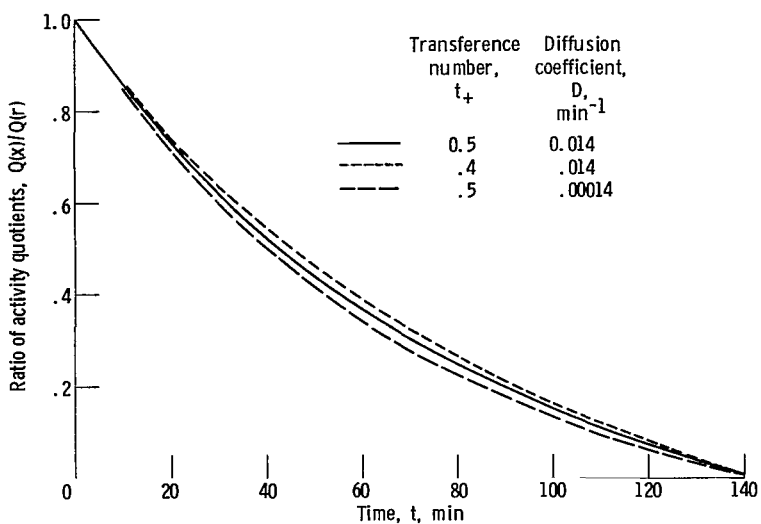


Figure 7. - Predicted dependence of activity quotient on time. Current, i , 0.030 A; volume of catholyte chamber, V_0 , 0.00109 liter.

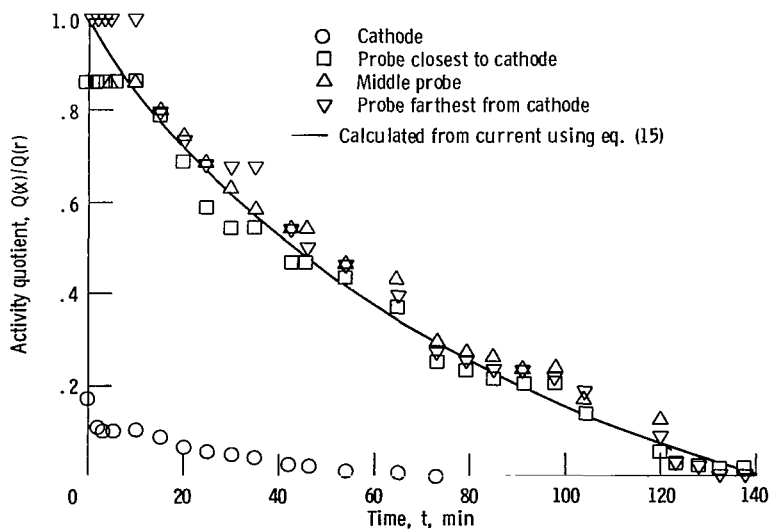


Figure 8. - Activity quotient in cathode chamber. Current, i , 0.030 A.

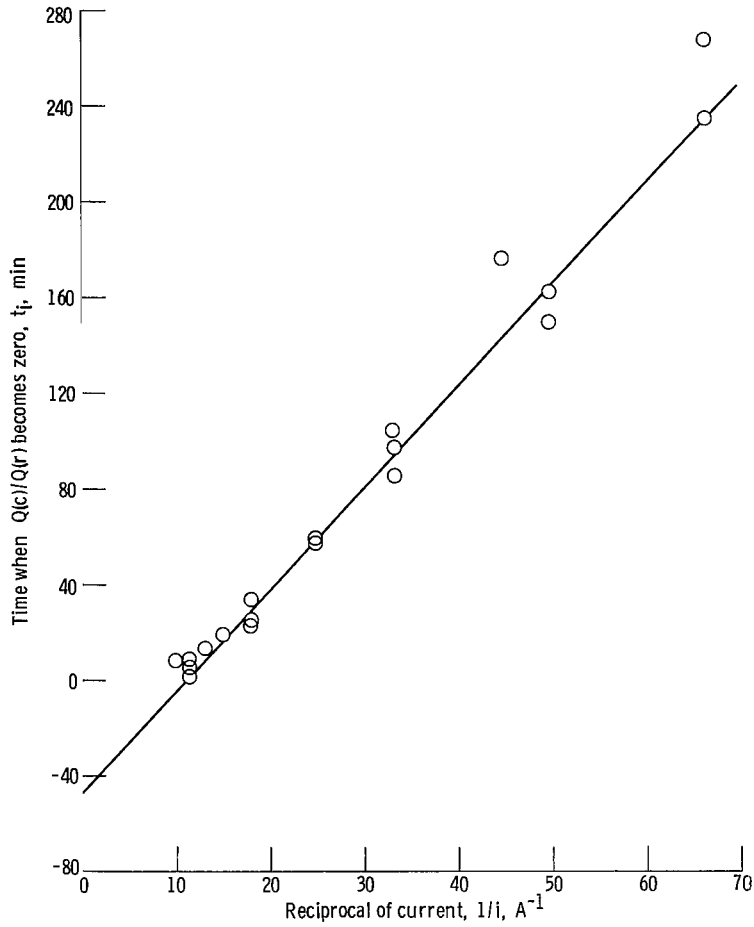
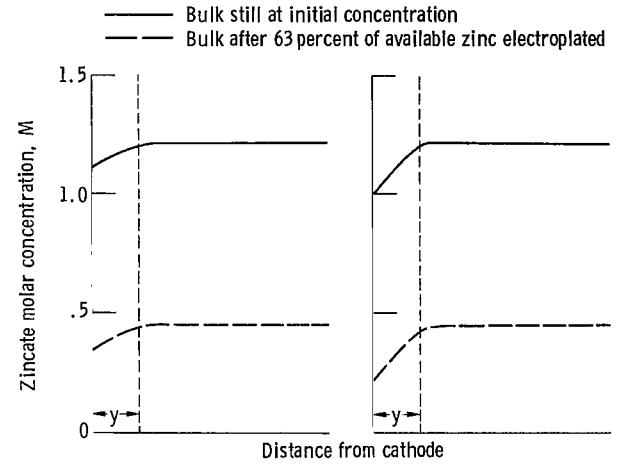
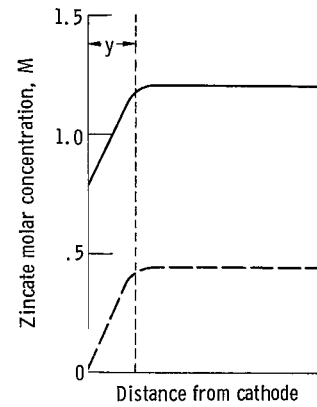


Figure 9. - Determination of proportionality constant γ_1 . $t_i = \frac{Z_0 V_0}{\theta i} - \frac{\gamma_1 V_0}{\theta}$.



(a) Current density, 0.010 A/cm².

(b) Current density, 0.020 A/cm².



(c) Current density, 0.040 A/cm².

Figure 10. - Zincate profiles for various current densities.

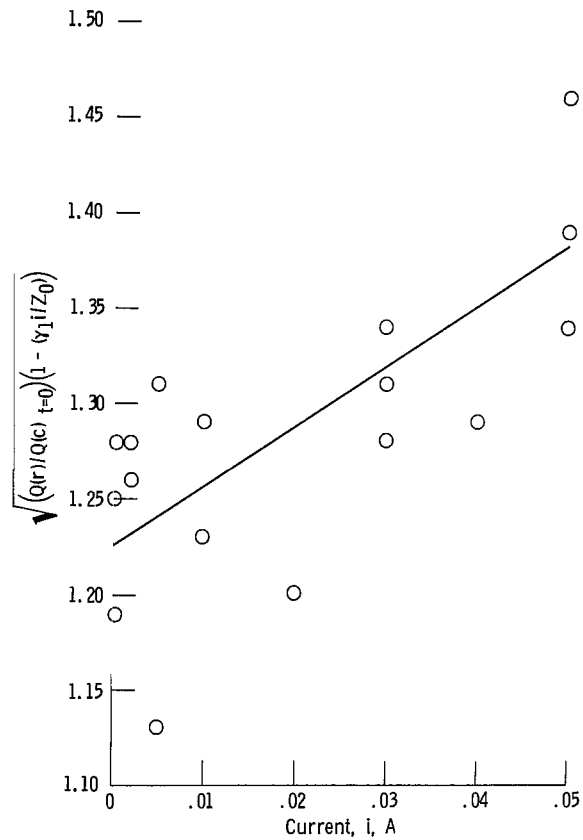


Figure 11. - Determination of apparent activity of mossy zinc M and proportionality constant γ_2 .

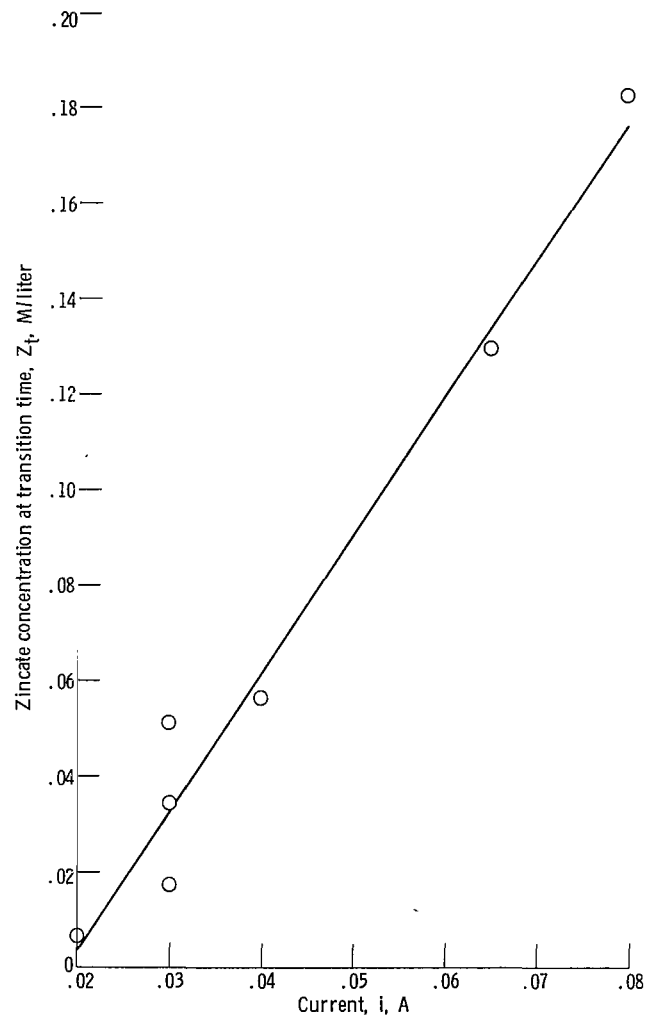


Figure 12. - Dependence of zincate concentration at transition time on current.

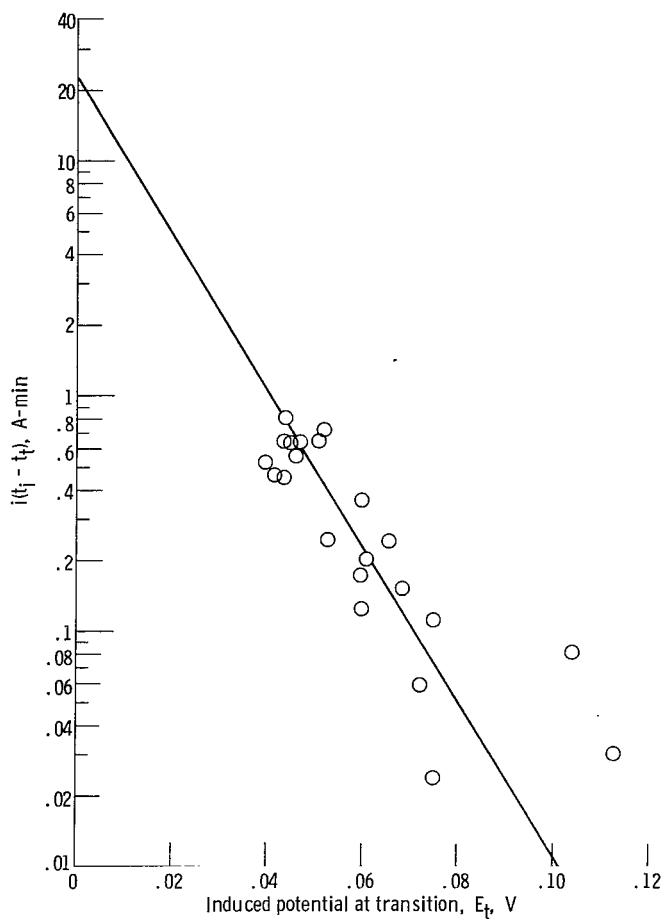


Figure 13. - Determination of $(H_t/H_0)(K_t/K_0)$ at transition time.

$$\ln i(t_j - t_t) = -\left(\frac{2F}{RT}\right) E_t + \ln \left[\left(\frac{H_t}{H_0}\right)^3 \left(\frac{K_t}{K_0}\right) \frac{MZ_0V_0}{\theta} \right].$$

NATIONAL AERONAUTICS AND SPACE ADMINISTRATION
WASHINGTON, D.C. 20546

OFFICIAL BUSINESS
PENALTY FOR PRIVATE USE \$300

**SPECIAL FOURTH-CLASS RATE
BOOK**

POSTAGE AND FEES PAID
NATIONAL AERONAUTICS AND
SPACE ADMINISTRATION
451



464 001 C1 U E 770701 S00903DS
DEPT OF THE AIR FORCE
AF WEAPONS LABORATORY
ATTN: TECHNICAL LIBRARY (SUL)
KIRTLAND AFB NM 87117

POSTMASTER: If Undeliverable (Section 158
Postal Manual) Do Not Return

"The aeronautical and space activities of the United States shall be conducted so as to contribute . . . to the expansion of human knowledge of phenomena in the atmosphere and space. The Administration shall provide for the widest practicable and appropriate dissemination of information concerning its activities and the results thereof."

—NATIONAL AERONAUTICS AND SPACE ACT OF 1958

NASA SCIENTIFIC AND TECHNICAL PUBLICATIONS

TECHNICAL REPORTS: Scientific and technical information considered important, complete, and a lasting contribution to existing knowledge.

TECHNICAL NOTES: Information less broad in scope but nevertheless of importance as a contribution to existing knowledge.

TECHNICAL MEMORANDUMS: Information receiving limited distribution because of preliminary data, security classification, or other reasons. Also includes conference proceedings with either limited or unlimited distribution.

CONTRACTOR REPORTS: Scientific and technical information generated under a NASA contract or grant and considered an important contribution to existing knowledge.

TECHNICAL TRANSLATIONS: Information published in a foreign language considered to merit NASA distribution in English.

SPECIAL PUBLICATIONS: Information derived from or of value to NASA activities. Publications include final reports of major projects, monographs, data compilations, handbooks, sourcebooks, and special bibliographies.

TECHNOLOGY UTILIZATION PUBLICATIONS: Information on technology used by NASA that may be of particular interest in commercial and other non-aerospace applications. Publications include Tech Briefs, Technology Utilization Reports and Technology Surveys.

Details on the availability of these publications may be obtained from:

SCIENTIFIC AND TECHNICAL INFORMATION OFFICE

NATIONAL AERONAUTICS AND SPACE ADMINISTRATION
Washington, D.C. 20546